Available online at www.sciencedirect.com

SciVerse ScienceDirect

Magnetic Resonance Imaging 30 (2012) 506–517

MAGNETIC RESONANCE IMAGING

Optimal real-time estimation in diffusion tensor imaging

Pablo Casaseca-de-la-Higuera[a, b,*], Antonio Tristán-Vega[a, b], Santiago Aja-Fernández[a], Carlos Alberola-López[a], Carl-Fredrik Westin[b], Raúl San José Estépar[b]

[a]*Laboratorio de Procesado de Imagen (LPI), Universidad de Valladolid, Valladolid, Spain*

[b]*Laboratory of Mathematics in Imaging (LMI), Brigham and Women's Hospital, Harvard Medical School, Boston MA, USA*

Received 20 May 2011; revised 24 October 2011; accepted 4 December 2011

Abstract

Diffusion tensor imaging (DTI) constitutes the most used paradigm among the diffusion-weighted magnetic resonance imaging (DW-MRI) techniques due to its simplicity and application potential. Recently, real-time estimation in DW-MRI has deserved special attention, with several proposals aiming at the estimation of meaningful diffusion parameters during the repetition time of the acquisition sequence. Specifically focusing on DTI, the underlying model of the noise present in the acquired data is not taken into account, leading to a suboptimal estimation of the diffusion tensor. In this paper, we propose an optimal real-time estimation framework for DTI reconstruction in single-coil acquisitions. By including an online estimation of the time-changing noise variance associated to the acquisition process, the proposed method achieves the sequential best linear unbiased estimator. Results on both synthetic and real data show that our method outperforms those so far proposed, reaching the best performance of the existing proposals by processing a substantially lower number of diffusion images.

Keywords: Diffusion tensor imaging; Real-time processing; Optimal sequential estimation; Best linear unbiased estimator (BLUE); Log-Rician distribution

1. Introduction

Magnetic resonance imaging (MRI) allows for easily identifying the anatomical structures of the brain in vivo. However, with this modality, the white matter appears as a homogeneous region, which hides the complex microarchitecture and connectivity of the nervous fibers comprised in this tissue. Diffusion-weighted MRI (DW-MRI) is intended to overcome this drawback, taking advantage of the diffusion of water molecules along the myelinated fiber bundles in the white matter.

The three-dimensional diffusion probability displacement function (PDF) or diffusion propagator of water molecules can be inferred from DW-MRI by acquiring a number of diffusion-sensitized images along different orientations of the sampling space. DW-MRI leads to diffusion-direction-dependent image intensities. In the case of anisotropic water diffusion, these intensities will be low if the measurement gradient direction is aligned with the major direction of diffusion and high for diffusion directions orthogonal to the measurement gradient direction.

The number of required diffusion-weighted images (DWIs) depends on how the diffusion is modeled. The well-known diffusion tensor (DT) model assumes a Gaussian PDF and requires at least six DWIs plus an additional unweighted image. Since the physics of the problem impose the radial symmetry of the diffusion, the entire process can be described in terms of the 3×3 covariance matrix of a Gaussian random variable. As such, the covariance matrix is positive, definite and symmetric, so it has only six degrees of freedom. This matrix is the diffusion tensor, and those techniques oriented to compute and represent it (or parameters derived from it) at each location of a three-dimensional volume are gathered under the denomination of DT (magnetic resonance) imaging (DT-MRI or DTI). Due to

* Corresponding author. ETSI Telecomunicación, Universidad de Valladolid. Camino del Cementerio s/n, 47011. Valladolid, Spain. Tel.: +34 983423660x5591; fax: +34 983423667.

E-mail addresses: casaseca@lpi.tel.uva.es (P. Casaseca-de-la-Higuera), atriveg@lpi.tel.uva.es (A. Tristán-Vega), sanaja@tel.uva.es (S. Aja-Fernández), caralb@tel.uva.es (C. Alberola-López), westin@bwh.harvard.edu (C.-F. Westin), rjosest@bwh.harvard.edu (R. San José Estépar).

0730-725X/$ – see front matter © 2012 Elsevier Inc. All rights reserved.
doi:10.1016/j.mri.2011.12.001

the six degrees of freedom of the DT, it may be determined from six independent gradient directions (thus, the need for six DWIs [1]). Nevertheless, it is very common to acquire a higher number of directions (DWIs) to improve the robustness of the estimation [2].

A number of techniques have been recently developed in order to overcome the limitations of the DT model. These limitations are imposed by the Gaussian assumption, which cannot properly model fiber bundle crossing (diffusion in two or more principal directions). The group of methods known as high angular resolution diffusion imaging (HARDI) goes beyond these limitations and ranges from more or less immediate extensions of the DT model to multitensor models [3–5], continuous distributions of tensors based on deconvolution approaches [6–10] or generalized tensor models [11], to even more general, nonparametric techniques [12,13] like the popular Q-ball [14,15] or the recent improvements including solid-angle considerations [16–18]. Recently, multishell approaches [18–20] have allowed to overcome some of the limitations of HARDI techniques at the expense of acquiring far more diffusion directions.

Robust estimation in DTI usually requires long acquisition times due to the increase in the number of DWIs needed. Acquisitions may be even longer for HARDI or multishell techniques [21,22]. This can be problematic when there is an excessive motion of the patient undergoing the scan (a frequent situation for neurological patients or children who cannot be sedated). Severe motion during the scan can force it to be aborted or render the acquired DWIs useless. Thus, one would like to make only as few acquisitions as possible. An estimation framework providing real-time estimates as new DWIs are available would allow online checking of the quality of the estimations. This would deliver immediate feedback to help the practitioner decide whether the acquisition is sufficiently acceptable to stop the procedure.

Poupon et al. [21,22] proposed an interesting approach based on the Kalman filter for real-time estimation of the DT and the orientation distribution function (ODF) obtained from Q-ball imaging. The DT model, provided that certain signal-to-noise ratio (SNR) conditions are met and no positivity constraints exist, is linear and easily fits into the Kalman filtering framework. As for the reconstruction of the ODF following [23], Deriche et al. [24] demonstrated that the approach in Refs. [21,22] was suboptimal and proposed a regularized Kalman filter that nicely addressed this issue. Brion et al. [25,26] recently proposed an improved version of the filters in Refs. [21,22,24]. In their work, the acquired DWIs are previously denoised in real time by means of the signal estimator proposed in Ref. [27]. This way, the Kalman filter benefits from the higher SNR of the observed data, yielding a performance improvement for both DT and ODF estimation.

The authors of Refs. [21,22], however, focus on the real-time aspect of the general algorithm, and thus, they do not elaborate on the specific noise statistics of the DT model. In their estimator, the same variance is considered for each logarithmic DWI signal (log-DWI hereafter), and this turns out not to be true [2,28]. With this constant variance assumption, the estimator proposed in Refs. [21,22] behaves as a sequential ordinary least squares (OLS) algorithm, which is suboptimal for this application. The method in Refs. [25,26] also behaves as a sequential OLS since it considers that the noise variance after signal restoration is the same for all the restored log-DWIs. If this assumption is not valid before signal denoising, it will remain the same for the restored data. Thus, the OLS is also suboptimal in this case.

The batch (offline) OLS estimator can be shown to be the best linear unbiased estimator (BLUE) for the linear model provided that the underlying noise is uncorrelated (with the same variance for each log-DWI) and has zero mean [29]. For single-coil acquisitions, where the signal can be modeled as Rician [30], the noise in each gradient image is assumed to be independent, but the variance suffers nonnegligible changes across log-DWIs. Salvador et al. [2] proposed an improvement to DT estimation in single-coil acquisitions based on LS. Since no constant variance can be assumed, those measurements with higher noise variance are less reliable. A strategy giving higher relevance (weight) to those samples with lower variance would be preferable instead. Thus, the proposal in Ref. [2] was based on the weighted least squares (WLS) estimator, which is in fact the BLUE under these conditions[1].

It can be demonstrated that the optimal weights for the WLS estimator are the inverses of the noise variances associated to each log-DWI measurement, so a formal noise characterization of the linearized DT model is necessary. In Ref. [2], this problem was solved by assuming that the variance of the logarithmic observations in the Rician model is inversely proportional to the squared amplitude of the corresponding DWI signal. Though the authors only provided empirical evidence, it is an excellent approach which has been analytically solved in Ref. [28]. When the data have been previously denoised, the noise characterization depends on the specific filter employed for restoration, although, in most practical cases, the dependence with the DWI amplitudes remains the same.

In this paper, we address the problem of optimal real-time estimation in single-coil DT-MRI acquisitions. A strategy based on real-time signal restoration is proposed to incorporate time-varying noise information to the online estimation process. Based on this strategy, we propose a sequential WLS estimation framework which can be used with either directly measured data or the real-time restored data as inputs, achieving the BLUE in both contexts. A comparative analysis over both synthetic and real data shows

[1] In the case of simultaneous acquisition and parallel reconstruction schemes (pMRI), the noise is no longer Rician [31–33], and the bias in WLS estimation is relevant as shown in Ref. [28]. Thus, although the WLS is still applicable, it is not the BLUE for pMRI schemes.

that the proposed estimators, respectively, outperform the so far proposed Kalman filters in Refs. [21,22] and Refs. [25,26] when either the acquired or the real-time-denoised DWIs are used for estimation.

2. Background

2.1. The DT model

The tensor model relates the unnoisy DWI signal A_i for each gradient direction i to the T2 baseline image A_o by using the well-known Stejskal–Tanner equation [34]:

$$A_i = A_0 exp\left(-b\mathbf{g}_i^T\mathbf{D}\mathbf{g}_i\right),\ 1\le i\le N \tag{1}$$

where $\mathbf{g}_i=[g_{ix}, g_{iy}, g_{iz}]^T$ are the N gradient directions, b is the diffusion weighting parameter and $\mathbf{D}$ is the DT, a second-order tensor. The model in Eq. (1) can be easily simplified by taking logarithms on both sides of the equation:

$$log(A_0) - log(A_i) = b\mathbf{g}_i^T\mathbf{D}\mathbf{g}_i \tag{2}$$

and by further developing the quadratic form, a simple linear equation can be obtained:

$$x_i = \mathbf{h}_i^T\mathbf{d} \tag{3}$$

where we define the log-attenuations as $x_i=\log(A_0/A_i)$ and $\mathbf{d}=[D_{xx}, D_{xy}, D_{xz}, D_{yy}, D_{yz}, D_{zz}]^T$ is the vector of the six unknown components of the DT. The i-th sensitization vector is defined as $\mathbf{h}_i=b[g_{ix}^2, 2g_{ix}g_{iy}, 2g_{ix}g_{iz}, g_{iy}^2, 2g_{iy}g_{iz}, g_{iz}^2]^T$. By rearranging all the N equations describing the intensities for a given voxel, the following linear system can be obtained:

$$\mathbf{x} = \mathbf{H}\mathbf{d} \tag{4}$$

where $\mathbf{x}$ represents the column vector containing the N log attenuations and $\mathbf{H}$ is the diffusion-sensitization matrix, whose rows are given by $\mathbf{h}_i^T$. The DT can be easily obtained by solving the system in Eq. (4). Since the tensor is symmetric, it has only six degrees of freedom. Thus, the system in Eq. (4) can be solved for N=6. However, the noisy nature of the DWIs turns the process of solving the linear system in Eq. (4) into an estimation problem. Thus, a higher number of gradients is usually necessary in order to decrease the variance of the estimated tensor.

Assuming that no motion or other artifacts exist, the main source of noise in MR images is thermal noise [35]. Under these conditions, the received signal M_i is the Rician distributed envelope of a complex Gaussian process [30]:

$$M_i = |A_i + n_i| \tag{5}$$

where $n_i=n_{c,i}+jn_{s,i}$ is a complex noise process whose real and imaginary parts are independent Gaussian processes with zero mean and variance σ^2. With A_i related to the DT by Eq. (1), the linearization of Eq. (5) can be performed by taking logarithm on both sides, leading to the following equation [2]:

$$\mathbf{y} = \mathbf{H}\mathbf{d} + \boldsymbol{\varepsilon} \tag{6}$$

where the vector of measured log-attenuations is given by $\mathbf{y}=[y_1, y_2,.., y_N]^T$ with $y_i=\log(A_0/M_i)$ distributed under a log-Rician probability law (see Ref. [2], Eqs. (13–14)) and $\boldsymbol{\varepsilon}$ is the vector of N independent noise terms. There are three important issues concerning this noise term that should be highlighted:

1. $E\{\boldsymbol{\varepsilon}\}\approx\mathbf{0}$.
2. The noise covariance ($\mathrm{Cov}\{\boldsymbol{\varepsilon}\}$) is given by

$$\mathbf{C}_{\boldsymbol{\varepsilon}} = \mathrm{diag}\left(\sigma_1^2, \sigma_2^2, \ldots, \sigma_N^2\right) \tag{7}$$

where $\sigma_i\approx\sigma/A_i$, i=1,... N.

3. For SNR values higher than 4 dB, the noise distribution is approximately Gaussian, i.e., $\boldsymbol{\varepsilon}\sim\mathcal{N}$ ($\mathbf{0}$, $\mathbf{C}\boldsymbol{\varepsilon}$).

Salvador et al. [2] provided empirical evidence of both the proximity to the Gaussian nature and the approximate values of the first- and second-order moments. As for the moment values, analytical expressions for the moments of $\log(M_i)$ are provided in Ref. [28]. From these equations, the derivation of the corresponding expressions for $\boldsymbol{\varepsilon}_i$ is straightforward.

2.2. Classical batch estimation in DTI

The simple model in Eq. (6) fits perfectly into an LS estimation framework. The OLS estimate of the vectorized DT is obtained as [29]:

$$\hat{\mathbf{d}} = \underset{\mathbf{d}}{\mathrm{argmin}}\left\{(\mathbf{y}-\mathbf{H}\mathbf{d})^T(\mathbf{y}-\mathbf{H}\mathbf{d})\right\} = \left(\mathbf{H}^T\mathbf{H}\right)^{-1}\mathbf{H}^T\mathbf{y} \tag{8}$$

The OLS estimator in Eq. (8) constitutes the de facto standard which is used in almost every clinical study based on DT-MRI. However, the linearized DT model resembles the type of model for which the WLS estimators are optimal (in terms of minimum variance and bias of the estimates). The OLS estimator coincides with the BLUE for the linear model in Eq. (6) if $E\{\boldsymbol{\varepsilon}\}=\mathbf{0}$ and $\mathbf{C}_{\boldsymbol{\varepsilon}}=\sigma_{OLS}^2\,\mathrm{I}_N$, with σ_{OLS}^2 a constant variance term for all i and $\mathbf{I}_N$ the $N\times N$ identity matrix. However, for the log-Rician model, $\mathbf{C}_{\boldsymbol{\varepsilon}}$ is given by Eq. (7). Thus, the BLUE in this case is the WLS estimator [29]:

$$\hat{\mathbf{d}} = \underset{\mathbf{d}}{\mathrm{argmin}}\left\{(\mathbf{y}-\mathbf{H}\mathbf{d})^T\mathbf{W}(\mathbf{y}-\mathbf{H}\mathbf{d})\right\} = \left(\mathbf{H}^T\mathbf{W}\mathbf{H}\right)^{-1}\mathbf{H}^T\mathbf{W}\mathbf{y} \tag{9}$$

with the optimal weight matrix given by $\mathbf{W}=\mathbf{C}_{\boldsymbol{\varepsilon}}^{-1}=\mathrm{diag}(1/\sigma_1^2, 1/\sigma_2^2,..., 1/\sigma_N^2)$. Since $\sigma_i=A_i/\sigma$ for the log-Rician model — Eq. (6) — a previous knowledge of the A_i values is necessary to estimate the DT applying WLS. However, at the beginning of

the estimation process, only the noisy M_i values are available. This problem can be solved by estimating the A_i values beforehand. Since the OLS estimates remain unbiased under inequality of variances, they can be used to give this preliminary estimate. Despite the necessity of this iterative estimation, the WLS constitutes an interesting alternative to OLS estimation in DTI. Apart from being the BLUE, if the Gaussian assumption for the measured signal can be made, the WLS is also an efficient estimator [29].

2.3. Real-time deterministic estimation: sequential least squares

Real-time deterministic estimation of the DT can be performed by sequentially processing the observed DWIs instead of waiting for all the available data. Specifically, assume we have determined the OLS (or the WLS) estimate $\widehat{\mathbf{d}}_{i-1}$ based on $\{y_1, y_2,\ldots, y_{i-1}\}$. If we now observe y_i, an updated $\widehat{\mathbf{d}}_i$ can be obtained without solving the linear Eq.(8) or (9). The procedure is termed *sequential least squares* to distinguish it from the original OLS and WLS (batch) approaches.

Considering the BLUE for the log-Rician case, the sequential update equations that lead to the minimization of the WLS error criterion $J_{WLS}=(\mathbf{y}-\mathbf{Hd})^T\,\mathbf{C}_{\boldsymbol{\varepsilon}}^{-1}\,(\mathbf{y}-\mathbf{Hd})$ are given by [29]

Estimator update:

$$\widehat{\mathbf{d}}_i = \widehat{\mathbf{d}}_{i-1} + \mathbf{k}_i\left(y_i - \mathbf{h}_i^T\,\widehat{\mathbf{d}}_{i-1}\right) \tag{10}$$

with

$$\mathbf{k}_i = \frac{\boldsymbol{\Sigma}_{i-1}\mathbf{h}_i}{\sigma_i^2 + \mathbf{h}_i^T\boldsymbol{\Sigma}_{i-1}\mathbf{h}_i} \tag{11}$$

Covariance update:

$$\boldsymbol{\Sigma}_i = \left(\mathbf{I}_p - \mathbf{k}_i\mathbf{h}_i^T\right)\boldsymbol{\Sigma}_{i-1} \tag{12}$$

where the gain factor $\mathbf{k}_i$ is a $p\times 1$ vector, with $p=6$ the dimension of the DT, and $\boldsymbol{\Sigma}_i$ is the covariance matrix of $\widehat{\mathbf{d}}_i$. Note that $\mathbf{k}_i$ has to be calculated before the estimator is updated, i.e., Eq. (11) is computed before Eq. (10). The sequential WLS estimator can only be obtained if the weight matrix is diagonal [29]. That is, the model noise must be uncorrelated, which is the case for the log-Rician model.

The update Eqs. (10–12) constitute the sequential WLS estimator, which is actually the sequential BLUE for the DT log-Rician model. The equations resulting from the sequential minimization of the OLS error criterion are the same as Eqs. (10–12), but for the constant variance term σ^2 (as opposed to σ_i^2) in Eq. (11).

To start the recursion in both estimators, we need to specify initial values for $\widehat{\mathbf{d}}_{i-1}$ and $\boldsymbol{\Sigma}_{i-1}$, so that $\mathbf{k}_i$ can be determined from Eq. (11) and then $\widehat{\mathbf{d}}_i$ from Eq. (10). A common practice is to get it started with a batch estimate based on $p=6$ observations where $\widehat{\mathbf{d}}_p$ is obtained from Eq. (9) for the WLS case or Eq. (8) for the OLS. The covariance matrix $\boldsymbol{\Sigma}_p$ is obtained as $\boldsymbol{\Sigma}_p=\mathbf{C}_{\widehat{\mathbf{d}}_p}=(\mathbf{H}^T\mathbf{W}\mathbf{H})^{-1}$ [29], where, in this case, the diffusion–sensitization matrix is constructed from p gradients. As stated before, the optimal weight matrix is $\mathbf{C}_{\boldsymbol{\varepsilon}}^{-1}$ in the WLS case, whereas for the OLS, $\mathbf{I}_p$ appears instead. An alternative method of initializing the recursion is to assign values for $\widehat{\mathbf{d}}_0$ and $\boldsymbol{\Sigma}_0$. This usually has the effect of biasing the estimator toward $\mathbf{d}_0$ [29]. Typically, to minimize the biasing effect, we choose $\boldsymbol{\Sigma}_0$ to be large (little confidence in $\widehat{\mathbf{d}}_0$) or $\boldsymbol{\Sigma}_0=\alpha\mathbf{I}_p$, where α is large compared to the typical eigenvalues of $\mathbf{d}$, and also $\widehat{\mathbf{d}}_0=\mathbf{0}$. This latter approach will be adopted here.

2.4. Limitations of the existing methods

In Refs. [21,22], a real-time DT estimator based on the Kalman filter was proposed. The Kalman filter constitutes an extension of the sequential linear minimum squared error (LMMSE) estimator to the case where the unknown parameter evolves in time according to a dynamical model. Considering the DT model, the parameter vector $\mathbf{d}$ is a constant. In this case, the implementation of the Kalman filter leads to the sequential LMMSE estimator which turns to a sequential LS estimator since no prior information on the tensor statistics is considered in the estimation problem (the Bayesian LMMSE estimator behaves as the deterministic LS). Moreover, in their proposal, Poupon et al. [21,22] do not fully address the true noise statistics of the signal model. Considering the model in Eq. (6), the formulation of the filter proposed in Refs. [21,22] is the same as the sequential estimator given by Eqs. (10–12) with $\sigma_i=1,\forall i$. Thus, the Kalman filter in Refs. [21,22] is actually the suboptimal sequential OLS, and its performance is, due to its own nature, bounded by that of the batch OLS.

The method in Refs. [25,26] is the same as the one in Refs. [21,22] except for the fact that an estimation of the unnoisy signal $\widehat{A}_i$ is used as the observation instead of the noisy M_i. That is, the linear model in Eq. (6) is constructed from the estimated signal levels as

$$\mathbf{y}^r = \mathbf{Hd} + \boldsymbol{\varepsilon}^r \tag{13}$$

where the vector of restored log-attenuations is given by $\boldsymbol{y}^r=[y_1^r, y_2^r,\ldots, y_N^r]^T$ with $y_i^r=\log(A_0/\widehat{A}_i)$ and $\boldsymbol{\varepsilon}^r$ is the vector of N independent noise terms. The characterization of the noise variance depends on the specific method used for signal restoration. For the estimator in Ref. [27] (the one used in Refs. [25,26]), Aja-Fernández et al. showed empirically that the output of the filter could approximately be considered as Rician, that is, the signal model in Eq. (5) applies as

$$\widehat{A}_i = |A_i + n_i^r| \tag{14}$$

where $n_i^r=n_{c,i}^r+jn_{s,i}^r$ is a complex noise process whose real and imaginary parts are independent Gaussian processes with zero mean and variance σ_r^2, with $\sigma_r<\sigma$ due to the restoration process. Thus, for logarithmic noise in Eq. (13) we have in most practical cases $E\{\boldsymbol{\varepsilon}^r\}=\mathbf{0}$ and $\mathbf{C}_{\boldsymbol{\varepsilon}^r}=\mathrm{diag}(\sigma_1^2, \sigma_2^2, \ldots, \sigma_N^2)$ with

$$\sigma_i \approx \sigma_r / A_i \tag{15}$$

which also shows a strong dependence of the noise variance with each DWI level. Thus, the sequential OLS used in Refs. [25,26] for the estimation of the DT from the restored data is also suboptimal. In order to obtain optimal sequential estimators for the DT model, the time (gradient)-changing noise variance must be included in the estimation equations. With proper estimates of the σ_i values, the BLUE — WLS — can be easily constructed. Since the variance levels depend on the unnoisy diffusion signals A_i ($\sigma_i \approx \sigma/A_i$ for measured data, $\sigma_i \approx \sigma_r/A_i$ for restored data), an estimation $\widehat{A_i}$ of these signals must be provided in real time.

3. Optimal estimation framework with real-time calculation of log-Rician noise levels

3.1. Overview of the proposal

The estimation framework proposed in this paper is based on the optimal sequential BLUE (WLS) obtained from Eqs. (10–12) (see Section 3). The sequential algorithm proposed for the estimation of the DT is thus the following:

1. Initialization: Set the initial values for $\widehat{\mathbf{d}}_0$ and $\mathbf{\Sigma}_0$.
2. For i=1,..., N, perform[2]:
   (a) Obtain a real-time estimation of the unnoisy signal $\widehat{A_i}$ following the procedure described in Section 3.2.
   (b) Use the obtained signal level to estimate the noise variance $\widehat{\sigma_i^2}$ as described in Section 3.2.
   (c) Use the variance estimation to compute the gain factor $\mathbf{k}_i$ using Eq. (11).
   (d) Update the DT estimator using:
      i. Eq. (10) if DT estimation is performed over directly measured data.
      ii. Eq. (10) substituting y_i by $y_i^r = log(A_0/\widehat{A_i})$ if DT estimation is performed over restored data.
   (e) Update the covariance term using Eq. (12).

3.2. Real-time estimation of the noise variance

In Ref. [27], an estimator based on the LMMSE[3] was proposed for restoration of DWI data, together with the empirical evidence described about the validity of Eq. (15). Due to its high performance and computational efficiency, we have adopted this method for optimal real-time estimation of the signal values in our experiments. In addition, this signal estimator is the one used in Refs. [25,26] for the signal restoration process preceding the estimation of the DT. The adopted method lets us obtain the signal level for a given voxel $A_i(\mathbf{x})$ from a closed-form analytical expression based on sample local moments of the measured signal $M_i(\mathbf{x})$. The (square) signal LMMSE estimator is obtained as

$$\widehat{A_i^2}(\mathbf{x}) = \langle M_i^2(\mathbf{x})\rangle - 2\widehat{\sigma^2} + \kappa(\mathbf{x})\left(M_i^2(\mathbf{x}) - \langle M_i^2(\mathbf{x})\rangle\right) \quad (16)$$

where $\langle\cdot\rangle$ denotes a sample estimator calculated in a neighborhood centered in $\mathbf{x}$, and $\kappa(\mathbf{x})$ is defined as

$$\kappa(\mathbf{x}) = \frac{1 - 4\widehat{\sigma^2}\left(\langle M_i^2(\mathbf{x})\rangle - \widehat{\sigma^2}\right)}{\langle M_i^4(\mathbf{x})\rangle - \langle M_i^2(\mathbf{x})\rangle^2} \quad (17)$$

where we have substituted the variance of the complex Gaussian process associated to the Rician envelope σ^2 by an estimator obtained from the given data: $\widehat{\sigma^2}$.

A detailed survey including performance evaluation of methods aimed at this variance estimation was presented in Ref. [36] with the additional proposal of overperforming approaches based on local statistics. Any one of these methods could be incorporated to our estimation framework. For our experiments, we have adopted the following estimator over the baseline:

$$\widehat{\sigma^2} = \frac{1}{2}\,\mathrm{mode}\left\{\langle M_0^2(\mathbf{x})\rangle\right\} \quad (18)$$

which has been shown to provide accurate estimations in an efficient way since no previous background segmentation is needed [36].

The size of the neighborhood is a parameter that must be selected by the user. A 7×7 neighborhood has been shown to provide accurate estimates for both $\widehat{A_i^2}$ and $\widehat{\sigma^2}$ with voxels whose side lengths were in the range 1.0–1.7 mm [27]. Thus, we have set this size for our experiments. The noise variance is finally calculated using Eqs. (16–17) for signal values and Eq. (18) for the variance of the complex Gaussian process as

$$\widehat{\sigma_i^2} = \widehat{\sigma^2} / \widehat{A_i^2} \quad (19)$$

if the DT is being estimated from the noisy measurements M_i or

$$\widehat{\sigma_i^2} = \widehat{\sigma_r^2} / \widehat{A_i^2} \quad (20)$$

for DT estimation over restored data using the LMMSE filter in Ref. [27]. As for the estimation of σ_r, we perform over the restored baseline as

$$\widehat{\sigma_r^2} = \frac{1}{2}\,\mathrm{mode}\left\{\langle A_0^2(\mathbf{x})\rangle\right\} \quad (21)$$

4. Experimental validation

4.1. Implementation details

4.1.1. Diffusion gradient orientation sets

The choice of diffusion orientation sets for DWI has been extensively studied in the literature. The standard procedure consists in acquiring N measurements that are uniformly

[2] N accounts for size of the diffusion gradient orientation set.

[3] Up to this point, we have referred to the LMMSE estimator of the DT. However, in this context, this concept applies to a different estimation problem, i.e., obtaining of the unnoisy A_i levels from the noisy M_i.

distributed in the unit sphere, so that the errors in measures derived from the DWIs are independent of tissue orientation. In the context of DWI, the problem of uniformly distributing has to be posed with symmetry constraints since a measure in the direction $\mathbf{g}=[g_x, g_y, g_z]^T$ is equivalent to a measurement in the direction $-\mathbf{g}$. However, the formulation of the problem is essentially the same. Some approaches have been proposed to undertake this problem with these symmetry constraints [37–39]. In fact, Ref. [39] publicly provides the optimal diffusion sets for $3\leq N\leq 150$ as part of the Camino Diffusion MRI Toolkit.

The approach in Ref. [39] yields optimized orientation sets when one considers all the diffusion acquisitions. However, if the acquisition is aborted before completion due to motion of the patient, the subset of orientations will be directionally biased and thus unusable for DT estimation [24]. Some algorithms for generating uniform point sets whose ordered subsets are also approximately uniform have been proposed [24,39,40]. With these algorithms, the acquired orientation sets for acquisitions aborted before completion are fairly uniform, and real-time estimation can be easily performed. All the methods perform in a similar way (see the comparison in Ref. [24], Section 4). Since the validation of the method in Refs. [21,22] was performed with the gradient orientation set proposed in Ref. [40], we will adopt this scheme in our experiments with synthetic data. Evaluation on real data will be performed by adopting the scheme in Ref. [24] since it allows for optimal reordering of existing orientation sets, is faster to implement and can be computed in real time.

4.1.2. Initialization issues and experimental setup

In any implementation of a sequential estimation algorithm, care must be taken in selecting proper initial conditions. In order to fairly compare with the closest approach [21,22], we will use the initialization constraints proposed in this work. Thus, the initial guesses $\widehat{\mathbf{d}}_0$ and $\mathbf{\Sigma}_0$ are, respectively, set to the null vector and the identity matrix. Since the eigenvalues of the DT typically lay close to 10^{-3}, this initialization provides little confidence on the initial estimate and thus avoids any bias toward $\widehat{\mathbf{d}}_0$.

In order to evaluate the proposed WLS estimators, we have performed some experiments over synthetically generated data under the log-Rician statistics. The algorithm in Refs. [21,22] and the one in Refs. [25,26] have also been evaluated for the sake of comparison. Since for isotropic diffusion the variance of the log-Rician noise remains constant across the DWIs (WLS ≡ OLS in this case), we have tested the behavior of both algorithms for nonisotropic tensors. Consequently, we used Eqs. (1) and (5) to synthesize the noisy DWIs from two nonisotropic tensors with eigenvalues $\lambda_i=[2\cdot10^{-3},\ 0.2\cdot10^{-3},\ 0.2\cdot10^{-3}]$ ($\lambda_1>\lambda_2=\lambda_3$, prolate tensor) and $\lambda_i=[1.1\cdot10^{-3},\ 1.1\cdot10^{-3},\ 0.2\cdot10^{-3}]$ ($\lambda_1=\lambda_2>\lambda_3$, oblate tensor). The scanner parameters were selected as b=1500 s/mm^2 and N=60 with the gradient orientation set proposed in Ref. [40]. Simulations have been performed for different SNR values ranging from 2 to 15 dB in 0.5-dB steps. The SNR has been calculated as $10\log_{10}(S^2/\sigma^2)$, with $S=\min(A_i)$. One thousand experiments have been carried out for each SNR value, with random orientation of the simulated tensors for each experiment.

We have also investigated the performance of the proposed scheme when estimating the DT from a real DWI volume. We use a SENSE EPI data set scanned in a General Electric 3.0-T Signa Excite Echospeed system with eight-channel head-coil (sequence: maximum gradient amplitudes, 40 mT/M; rectangular field of view of 220×165 mm; slice thickness, 1.7 mm; receiver bandwidth, 6 kHz; echo time, 70 ms; repetition time, 2500 ms). It comprises 8 nonweighted baseline images and 51 gradient directions — distributed on the sphere using the electric repulsion model with antipodal pairs [37,38] — which have been reordered for optimal sequential estimation following Ref. [24]. The voxel dimension is 0.9375×0.9375×1.7 mm^3 with an image matrix size of 256×256 and 81 slice locations. The b-value for the

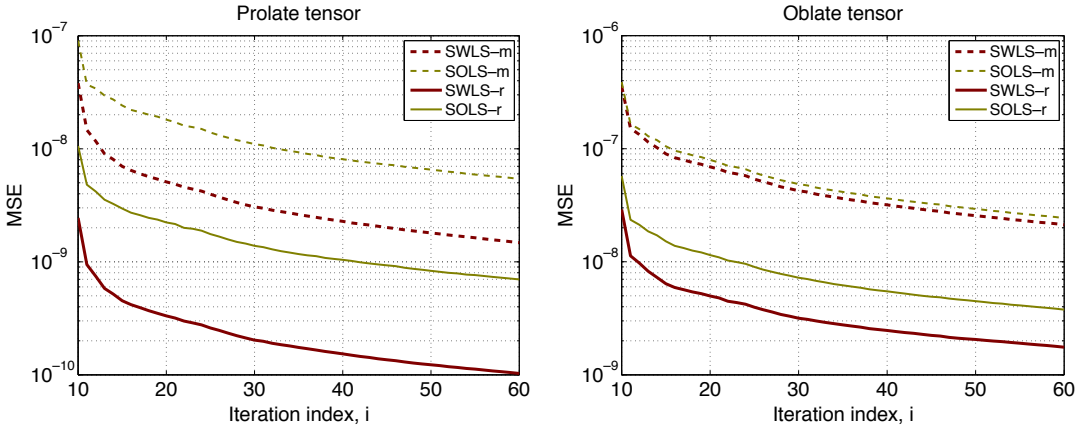

Fig. 1. MSE of the estimation vs. iteration index (i=10,…, 60) for simulated prolate (left) and oblate (right) tensors with SNR values ranging from 2 to 15 dB. Legend keys: SWLS-m: proposed sequential WLS estimator operating over directly measured data; SOLS-m: sequential OLS estimator operating over directly measured data (Kalman filter in Refs. [21,22]); SWLS-r: proposed sequential WLS estimator operating over restored data; SOLS-r: sequential OLS estimator operating over restored data (Kalman filter in Refs. [25,26]).

DWI acquisition is set to b=586 s/mm^2. We aim at extending the covered range of acquisition conditions by employing different values for the synthetic (b=586 s/mm^2) and in vivo (b=1500 s/mm^2) experiments. The value used for the latter is closer to the one used in Refs. [21,22] for DT estimation. This guarantees a fair comparison under conditions considered therein, which correspond to high SNR values. On the other hand, synthetic data were generated using b=1500 s/mm^2 in order to illustrate the performance of our proposal in situations where high angular contrast is needed and, thus, higher b-values are necessary. This way, low SNR conditions are also considered since this selection leads to higher attenuations of the diffusion images.

4.2. Results and discussion

4.2.1. Synthetic data

In Fig. 1, the mean square error (MSE) of the estimation has been plotted vs. the iteration index i=10,…, 60 considering all the SNR values on average. The error has been computed as the norm of the difference between the actual estimate for iteration i ($\widehat{\mathbf{d}}_i$) and the real value $\mathbf{d}$. Results for directly measured data reveal a higher performance of the proposed sequential WLS estimator (SWLS-m in figure legend) as compared with the OLS estimator (SOLS-m, the Kalman filter proposed in Refs. [21,22]). As for the estimation from real-time restored data, the proposed method (SWLS-r in figure legend) also outperforms the Kalman filter presented in Refs. [25,26] (SOLS-r), with a more noticeable performance improvement in this case.

The analysis of the results in Fig. 1 leads to the following conclusions:

- Our algorithms achieve the highest performance reached by the so far proposed Kalman filters [21,22,25,26], with a reduced number of acquisitions. This highest performance coincides with the one of the batch OLS estimator in both cases (directly measured and restored data) and is obtained for N=60 iterations. Considering the estimation of prolate tensors from directly measured data, our WLS outperforms the batch OLS before acquiring the 20th DWI. This means that the method in Refs. [21,22] needs at least 40 DWIs more to perform as ours. If we consider the estimation of prolate tensors from real-time restored data, the

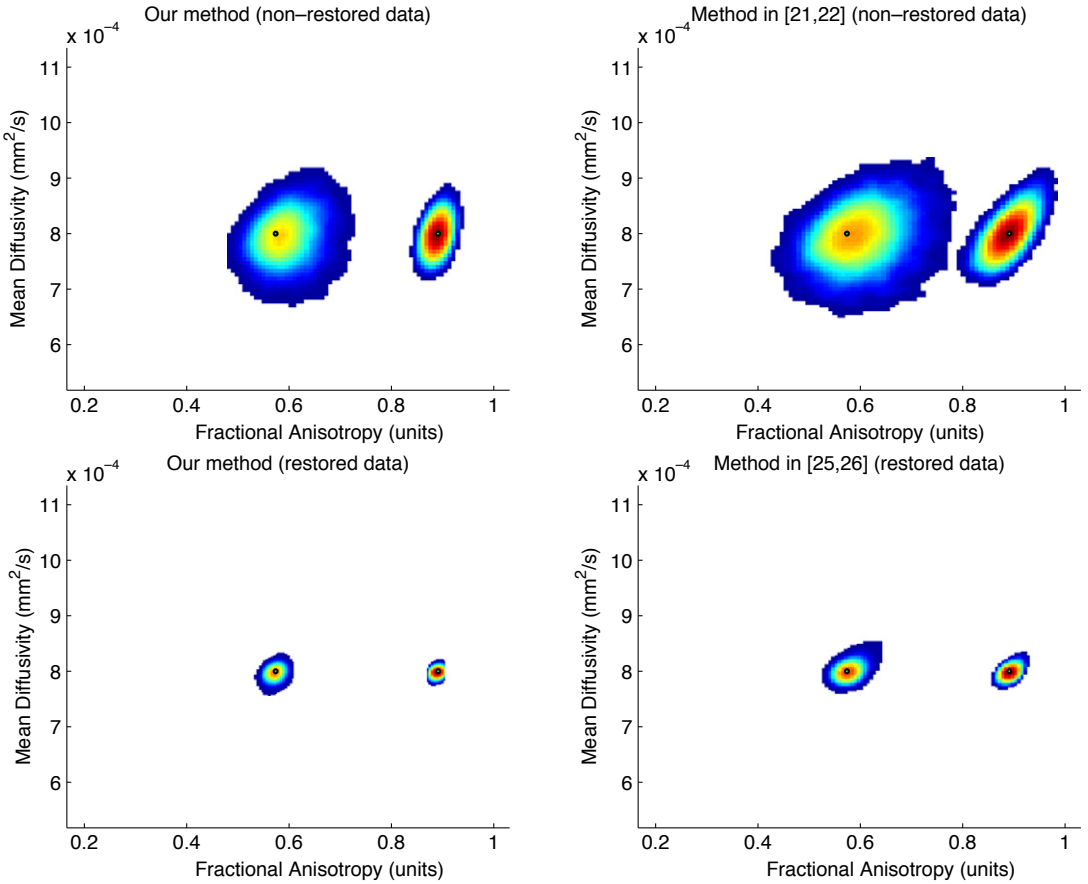

Fig. 2. Two-dimensional histograms of the distribution of the pairs (FA, MD) from the proposed algorithms (left) and the methods in Refs. [21,22] and Refs. [25,26] (right). Distributions for nonrestored data are shown in the upper part of the figure, while the lower part shows those for restored data. Results are presented for iteration i=15. Ground truth centroids are represented as green dots.

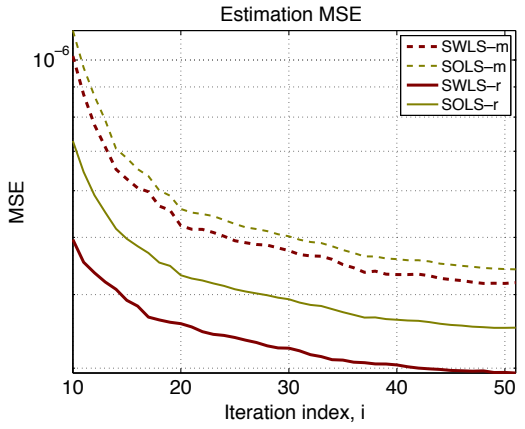

Fig. 3. MSE of the estimation vs. iteration index (i=10,..., 51) for the acquired in vivo volume. Legend keys: SWLS-m: proposed sequential WLS estimator operating over directly measured data; SOLS-m: sequential OLS estimator operating over directly measured data (Kalman filter in Refs. [21,22]); SWLS-r: proposed sequential WLS estimator operating over restored data; SOLS-r: sequential OLS estimator operating over restored data (Kalman filter in Refs. [25,26]).

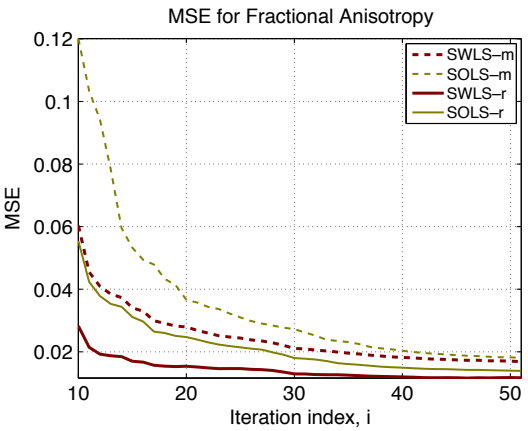

Fig. 4. MSE of FA vs. iteration index (i=10,..., 51) for the acquired in vivo volume. Legend keys: SWLS-m: proposed sequential WLS estimator operating over directly measured data; SOLS-m: sequential OLS estimator operating over directly measured data (Kalman filter in Refs. [21,22]); SWLS-r: proposed sequential WLS estimator operating over restored data; SOLS-r: sequential OLS estimator operating over restored data (Kalman filter in Refs. [25,26]).

estimation error obtained with our method equals that of the batch OLS at the 12th DWI, that is, the method in Refs. [25,26] needs 48 more acquisitions to equal the performance of our sequential WLS.

- The higher performance of our algorithms is more noticeable for prolate tensors, especially when data restoration is performed during the estimation process. For oblate tensors, differences exist, but they are lighter, especially for the unrestored case; in this scenario, the iteration at which our algorithm reaches the performance of the batch OLS lays between i=45 and i=50. However, on real-time restored data, the performance improvement is higher since the batch OLS performance is reached at the 25th DWI.
- The higher performance for prolate tensors can be explained as follows: By considering the time-varying noise variance, our algorithms tend to behave as the optimal WLS. On the other hand, the performance of the methods in Refs. [21,22] and Refs. [25,26] will always be below that of the OLS since a constant variance is assumed. When prolate tensors are to be estimated, the differences between WLS and OLS are even more pronounced. The main reason is that the noise variance has higher variability for prolate tensors, which is due to the abrupt changes that the DWI values A_i suffer along the acquisition process[4].
- Finally, the figures show that the differences between the sequential WLS and OLS estimators are more noticeable when real-time signal restoration is performed during the estimation process; this can be interpreted as follows: when the DWIs are previously denoised, the estimation of the DT is performed on observations with higher SNR. The main difference between the OLS and WLS estimation strategies resides in the fact that WLS estimation uses the inverse of the noise variance as a weighting term. The inverse function is very much

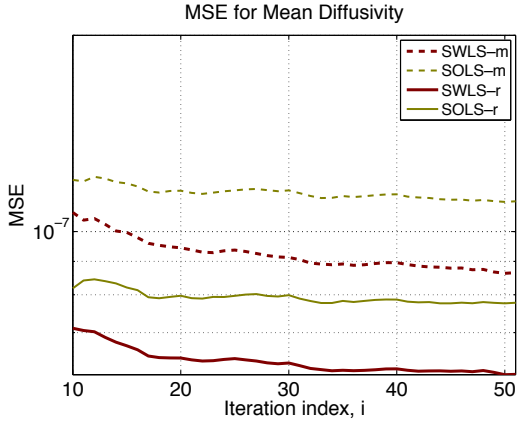

Fig. 5. MSE of MD vs. iteration index (i=10,..., 51) for the acquired in vivo volume. Legend keys: SWLS-m: proposed sequential WLS estimator operating over directly measured data; SOLS-m: sequential OLS estimator operating over directly measured data (Kalman filter in Refs. [21,22]); SWLS-r: proposed sequential WLS estimator operating over restored data; SOLS-r: sequential OLS estimator operating over restored data (Kalman filter in Refs. [25,26]).

[4] For prolate tensors, the main eigenvector determines the signal attenuation A_i/A_0. If this eigenvector is aligned with a specific gradient, the attenuation is maximal, and A_i will be close to 0. If, on the other hand, both vectors are orthogonal, minimal attenuation is achieved, and A_i will be close to A_0. This involves a high variability of $\sigma_i \propto \frac{1}{A_i}$ along the whole acquisition process.

nonlinear for smaller variances, so differences with OLS are more noticeable there.

As an illustration, the distribution of two tensor invariants, the mean diffusivity (MD) and the fractional anisotropy (FA), is depicted in two-dimensional histograms for iteration index i=15 (Fig. 2). The MD for both simulated tensors is $0.8 \cdot 10^{-3}$ mm^2/s. As for the FA, we have FA=0.8911 (prolate tensor) and FA=0.5738 (oblate). These original values are depicted as green dots

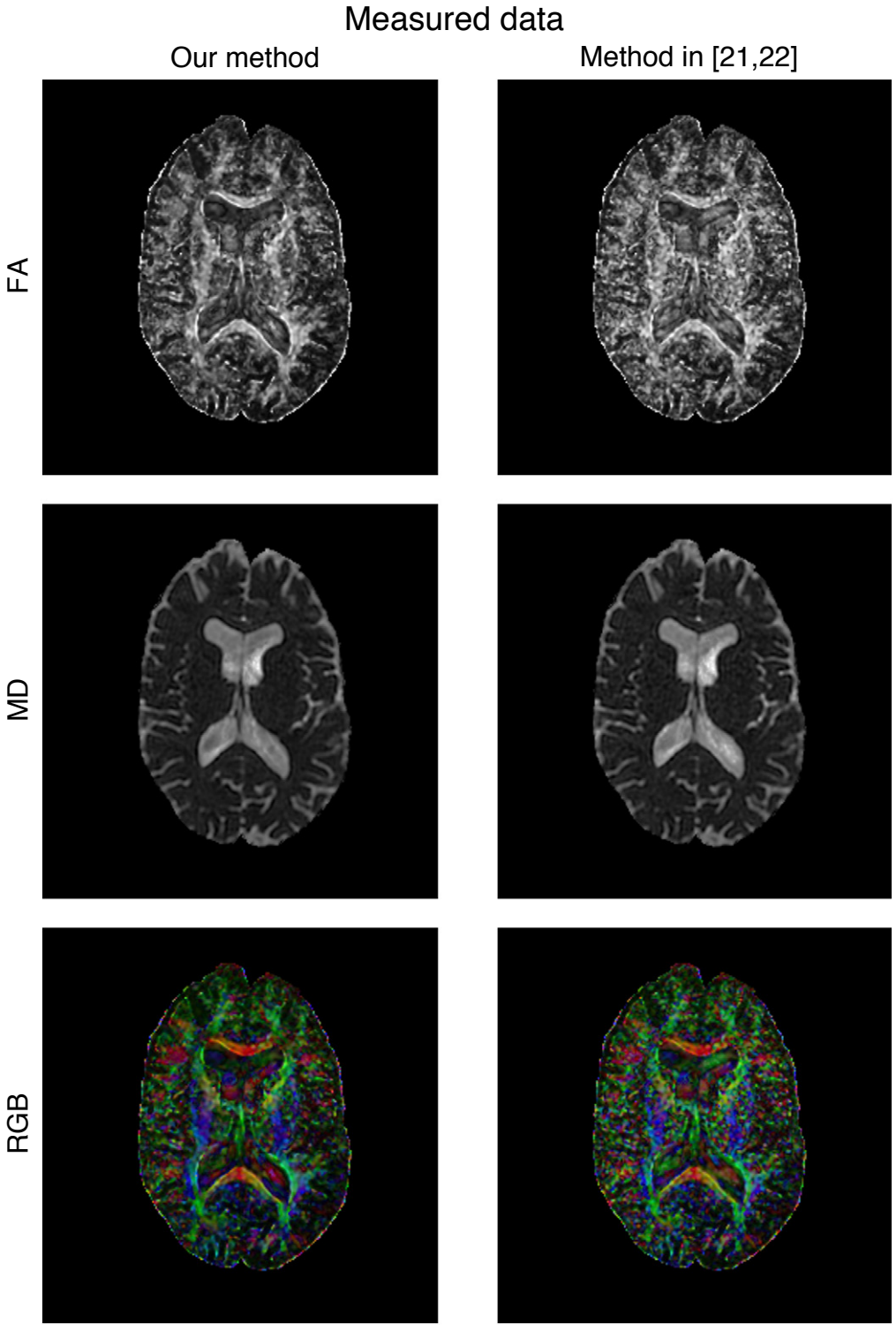

Fig. 6. FA, MD and RGB maps (slice #40 of the data set) estimated over directly measured data using our proposal (left) and the one in Refs. [21,22] (right) at iteration i=10.

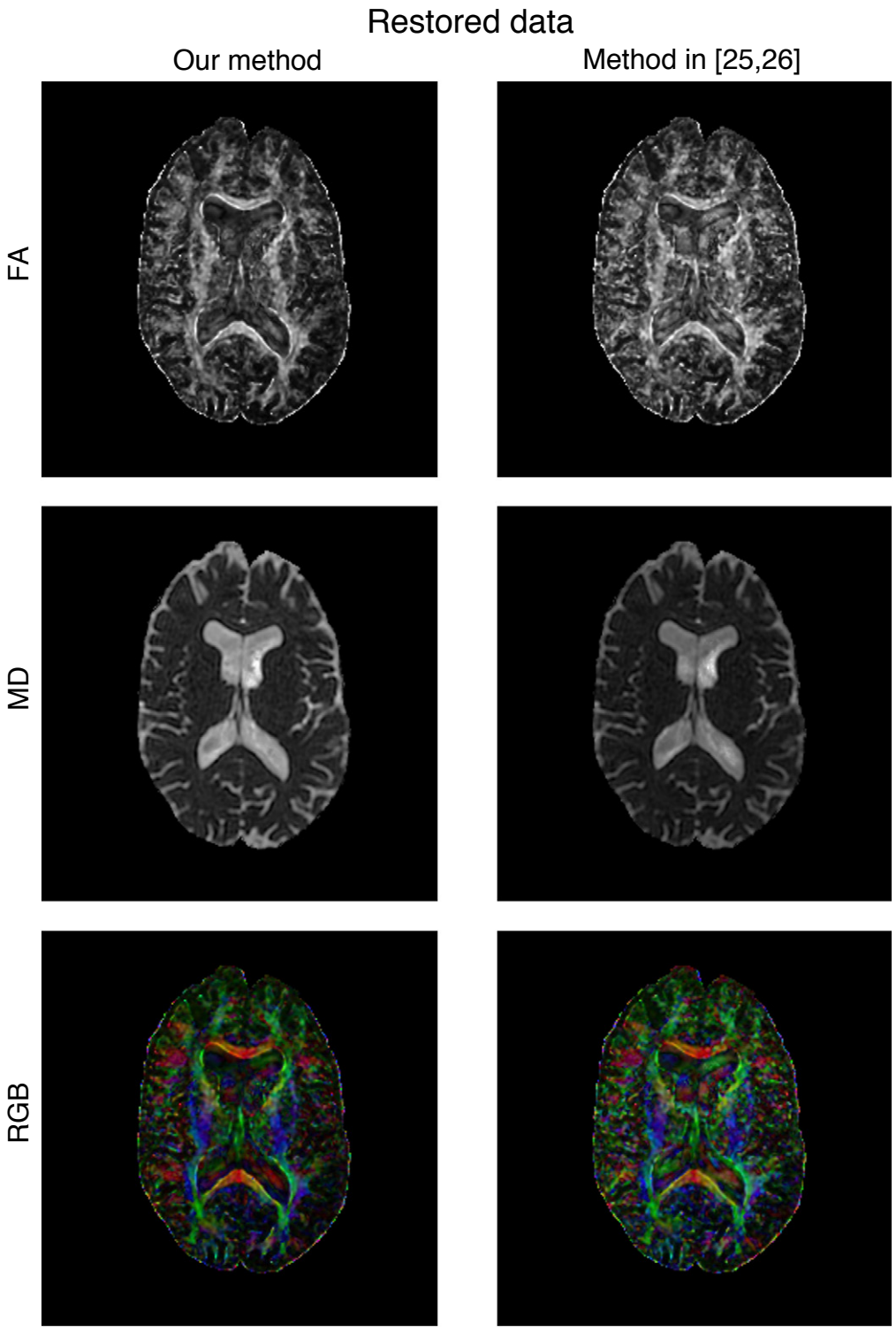

Fig. 7. FA, MD and RGB maps (slice #40 of the data-set) estimated over restored data using our proposal (left) and the one in Refs. [25,26] (right) at iteration i=10.

in Fig. 2. The upper and lower parts of Fig. 2 reveal a respective improvement in both bias and variance obtained from our methods in comparison to those in Refs. [21,22] and Refs. [25,26].

4.2.2. Real data

The MSE of the estimation vs. the iteration index i=10,..., 51 is presented in Fig. 3 for the real data set. The error has been computed from the DT estimation as in

Section 1, considering as a ground truth the batch WLS estimation for N=51 calculated over the same volume which was previously filtered with the joint LMMSE[5] filter proposed in Ref. [41]. Our method outperforms those previously proposed as can be inferred from the figure, with a more noticeable improvement when the estimation is performed over restored data.

The quantitative comparison between our method and those in Refs. [21,22,25,26] has also been performed in terms of FA and MD. Fig. 4 shows the MSE obtained from FA, while MD results are shown in Fig. 5. The higher performance of our method can be observed in both cases. However, the evolution of the performance improvement during the acquisition is different for both magnitudes. With respect to the FA, the performance of the sequential OLS estimators in Refs. [21,22] and Refs. [25,26] tends to converge to the one obtained from our method as the number of processed DWIs increases. As for the MD, such a convergence is not clearly appraised.

As a concluding illustration, Fig. 6 shows the FA, MD and RGB maps for the central slice (#40) of the data set obtained from application of our method over directly measured data at iteration index i=10. The maps obtained from the method in Refs. [21,22] are also presented for the sake of comparison. Finally, Fig. 7 represents the counterpart of Fig. 6 when real-time restoration is performed during estimation (maps obtained with the method in Refs. [25,26] are also presented). Results indicate a less spotty result with our algorithm using both the unfiltered and filtered data. The color representation makes this effect more pronounced due to the higher sensitivity of the human visual system to colors than to gray levels.

5. Conclusion

We have proposed an optimal real-time estimation framework for the DT in DWI acquisitions following the log-Rician noise model. Within this framework, the estimation of the DT can be performed even when the data are real-time restored. By considering the changes that the noise variance suffers across DWIs, our estimation methodology implements the optimal BLUE for both directly measured and real-time restored data. In order to estimate the time-changing noise variance, the unnoisy diffusion levels are additionally needed in real time. Our method includes a simple LMMSE estimator for these signal levels which can be easily incorporated to the real-time framework since it is based on local sample statistics.

Results on both synthetic and real data have shown that our method outperforms the so far proposed (Refs. [21,22] for measured data and Refs. [25,26] for real-time denoised data). These methods are suboptimal for the log-Rician (denoised log-Rician) model since they assume the same noise variance for each log-DWI (restored log-DWI) and, thus, their performance is the same as the sequential OLS. Our framework incorporates the specific noise statistics of the acquired or denoised data to the estimation process, leading to the implementation of optimal estimators.

Real-time estimation constitutes an important tool in DWI acquisition either for tuning up the diffusion parameters or as a feedback source of information on the acquisition process. Currently, due to time restrictions, DWI data acquisitions are usually accelerated by using parallel MRI (pMRI) reconstruction techniques, which allow increasing the acquisition rate via subsampled acquisitions of the **k**-space. The development of optimal real-time estimators specifically focused on pMRI schemes constitutes a challenging task, mainly due to the following factors: (1) The underlying noise model is not as simple as in single-coil acquisitions since spatial nonstationarities do exist. (2) Those optimal estimators for the log-Rician model are suboptimal for some pMRI reconstruction schemes such as the fully sampled sum of squares [32] or the generalized autocalibrating partially parallel acquisitions scheme [42]. (3) The data to be processed at each iteration of the acquisition multiply by the number of coils, thus limiting the real-time nature of the estimator. (4) The acceleration schemes for image reconstruction constitute an additional limitation for real-time estimation since they reduce the available time for online processing. Currently, we are investigating the possibility of developing real-time optimal estimators under these scenarios.

Acknowledgments

This work was partially supported by the Ministerio de Ciencia e Innovación and the Fondo Europeo de Desarrollo Regional (FEDER) under Research Grant TEC2010-17982 and by the Centro para el Desarrollo Tecnológico Industrial (CDTI) under the cvREMOD (CEN-20091044) project. The work was also funded by the Junta de Castilla y León under Grants VA376A11-2 and VA039A10-2. A. Tristán-Vega was supported by FMECD-2010/71131616E (Ministerio de Educacíon, Spain/Fulbright Committee). C.-F. Westin was supported by NIH grants R01MH074794, R01MH092862, and P41RR013218. R. San José was supported by NIH award number K25HL104085. The authors would also like to acknowledge the company Q Diagnóstica for the research agreement with the University of Valladolid (2011–2013), through which most MRI acquisitions of the LPI are currently obtained.

References

[1] Basser PJ, Pierpaoli C. Microstructural and physiological features of tissues elucidated by quantitative-diffusion-tensor MRI. J Magn Reson 1996;111(3):209–19.

[5] In this context, the estimation problem also deals with obtaining the A_i levels from the noisy M_i.

[2] Salvador R, Peña A, Menon DK, Carpenter TA, Pickard JD, Bullmore ET. Formal characterization and extension of the linearized diffusion tensor model. Hum Brain Mapp 2005;24:144–55.
[3] Kreher BW, Schneider JF, Mader I, Martin E, Henning J, Il'yasov KA. Multitensor approach for analysis and tracking of complex fiber configurations. Magn Reson Med 2005;54(5):1216–25.
[4] Peled S, Friman O, Jolesz F, Westin CF. Geometrically constrained two-tensor model for crossing tracts in DWI. Magn Reson Med 2006;24(9):1263–70.
[5] Bergmann Ø, Kindlmann G, Lundervold A, Westin CF. Diffusion k-tensor estimation from Q-ball imaging using discretized principal axes. Medical Image Computing and Computer-Assisted Intervention, vol. 4191 of Lecture Notes in Computer Science. Springer–Verlag; 2007. p. 268–75.
[6] Anderson AW. Measurement of fiber orientation distributions using high angular resolution diffusion imaging. Magn Reson Med 2005;54 (5):1194–206.
[7] Descoteaux M, Deriche R, Knösche TR, Anwander A. Deterministic and probabilistic tractography based on complex fibre orientation distributions. IEEE Trans Med Imaging 2009;28(2):269–86.
[8] Jian B, Vemuri BC, Özarslan E, Carney PR, Marecy TH. A novel tensor distribution model for the diffusion-weighted MR signal. NeuroImage 2007;37(1):164–76.
[9] Tournier JD, Calamante F, Connelly A. Robust determination of the fibre orientation distribution in diffusion MRI: non-negativity constrained super-resolved spherical deconvolution. NeuroImage 2007;35:1459–72.
[10] Tournier JD, Yeh CH, Calamante F, Cho KH, Connelly A, Lin CP. Resolving crossing fibres using constrained spherical deconvolution: validation using diffusion-weighted imaging phantom data. NeuroImage 2008;42:617–25.
[11] Descoteaux M, Angelino E, Fitzgibbons S, Deriche R. Apparent diffusion profile estimation from high angular resolution diffusion images: estimation and applications. Magn Reson Med 2006;56(2):395–410.
[12] Jansons KM, Alexander DC. Persistent angular structures: new insights from diffusion magnetic resonance imaging data. Inverse Probl 2003;19:1031–46.
[13] Özarslan E, Sepherd TM, Vemuri BC, Blackband SJ, Mareci TH. Resolution of complex tissue microarchitecture using the diffusion orientation transform (DOT). NeuroImage 2006;31:1086–103.
[14] Tuch DS, Reese T, Wiegell MR, Wedeen VJ. Diffusion MRI of complex neural architecture. Neuron 2003;40:885–95.
[15] Tuch DS. Q-ball imaging. Magn Reson Med 2004;52:1358–72.
[16] Tristán-Vega A, Westin CF, Aja-Fernández S. Estimation of fiber orientation probability density functions in high angular resolution diffusion imaging. NeuroImage 2009;47:638–50.
[17] Tristán-Vega A, Westin CF, Aja-Fernández S. A new methodology for the estimation of fiber populations in the white matter of the brain with the Funk–Radon transform. NeuroImage 2010;49:1301–15.
[18] Aganj I, Lenglet C, Sapiro G, Yacoub E, Ugurbil K, Harel N. Reconstruction of the orientation distribution function in single and multiple shell Q-ball imaging within constant solid angle. Mag Res Med 2010;64(2):554–66.
[19] Wu Y-C, Field A, Alexander L. Computation of diffusion function measures in q-space using magnetic resonance hybrid diffusion imaging. IEEE Trans Med Imaging 2008;27(6):858–65.
[20] Canales-Rodríguez EJ, Melie-García L, Iturria-Medina Y. Mathematical description of q-space in spherical coordinates: exact Q-ball imaging. Magn Reson Med 2009;61:1350–67.
[21] Poupon C, Poupon F, Roche A, Cointepas Y, Dubois J, Mangin J. Real-time MR diffusion tensor and Q-ball imaging using Kalman filtering. Medical Image Computing and Computer-Assisted Intervention, Lecture Notes in Computer Science. Springer–Verlag; 2007. p. 27–35.
[22] Poupon C, Roche A, Dubois J, Mangin JF, Poupon F. Real-time MR diffusion tensor and Q-ball imaging using Kalman filtering. Med Image Anal 2008;12(5):527–34.
[23] Descoteaux M, Angelino E, Fitzgibbons S, Deriche R. Regularized, fast, and robust analytical Q-ball imaging. Magn Reson Med 2007;58: 497–510.
[24] Deriche R, Calder J, Descoteaux M. Optimal real-time Q-ball imaging using regularized Kalman filtering with incremental orientation sets. Medical Image Anal 2009;13(4):564–79.
[25] Brion V, Kezele I, Riff O, Descoteaux M, Mangin JF, Poupon C, et al. Real-time Rician noise correction applied to real-time HARDI and HYDI. MICCAI 2010 Workshop on Computational Diffusion MRI (CDMRI 2010); 2010. p. 4–13.
[26] Brion V, Riff O, Kezele I, Descoteaux M, Le Bihan JF, Mangin D, et al. Real-time Rician noise correction applied to real-time HARDI and HYDI. Proceedings of the International Society of Magnetic Resonance in Medicine (ISMRM 2011), Vol. 19; 2011. p. 1930.
[27] Aja-Fernández S, Niethammer M, Kubicki M, Shenton ME, Westin CF. Restoration of DWI data using a Rician LMMSE estimator. IEEE Trans Med Imaging 2008;27(10):1389–403.
[28] Tristán-Vega A, Westin CF, Aja-Fernández S. Bias of least squares approaches for diffusion tensor estimation from array coils in DT-MRI. Medical Image Computing and Computer-Assisted Intervention, Lecture Notes in Computer Science. Springer–Verlag; 2009. p. 919–26.
[29] Kay SM. Fundamentals of statistical signal processing. Estimation theory. Upper Saddle River (NJ): Prentice–Hall; 1993.
[30] Gudbjartsson H, Patz S. The Rician distribution of noisy MRI data. Magn Reson Med 1995;34:910–4.
[31] Roemer PB, Edelstein WA, Hayes CE, Souza SP, Mueller OM. The NMR phased array. Magn Reson Med 1990;16:192–225.
[32] Constantinides CD, Atalar E, McVeigh ER. Signal-to-noise measurements in magnitude images from NMR phased arrays. Magn Reson Med 1997;38:852–7.
[33] Gilbert G, Simard D, Beaudoin G. Impact of an improved combination of signal from array coils in diffusion tensor imaging. IEEE Trans Med Imaging 2007;26(11):1428–36.
[34] Stejskal EO, Tanner JE. Spin diffusion measurements: spin echoes in the presence of a time-dependent field gradient. J Chem Phys 1965;42: 288–92.
[35] Haacke EM, Brown RW, Thomson MR, Venkatesan R. Magnetic resonance imaging: physical principles and sequence design. New York: Wiley; 1999.
[36] Aja-Fernández S, Tristán-Vega A, Alberola-López C. Noise estimation in single and multiple coil MR data based on statistical models. Magn Reson Imaging 2009;27:1397–409.
[37] Jones D, Horsfield M, Simmons A. Optimal strategies for measuring diffusion in anisotropic systems by magnetic resonance imaging. Magn Reson Med 1999;43(3):515–25.
[38] Papadakis N, Murrills C, Hall L, Huang C, Carpenter T. Minimal gradient encoding for robust estimation of diffusion anisotropy. Magn Reson Imaging 2000;18(6):671–9.
[39] Cook P, Symms M, Boulby P, Alexander D. Optimal acquisition orders of diffusion-weighted MRI measurements. J Magn Reson Imaging 2007;26(5):1051–8.
[40] Dubois J, Poupon C, Lethimonnier F, Bihan D. Optimized diffusion gradient orientation schemes for corrupted clinical DTI data sets. MAGMA 2006;19(3):134–43.
[41] Tristán-Vega A, Aja-Fernández S. DWI filtering using joint information for DTI and HARDI. Med Image Anal 2010;14:205–18.
[42] Griswold MA, Jakob PM, Heidemann RM, Nittka M, Jellus V, Wang J, et al. Generalize autocalibrating partially parallel acquisitions (GRAPPA). Magn Reson Med 2002;47:1202–10.